Electromagnetic Analysis and Optimization for a Dual-Rotor Switched Reluctance Machine

Xing Wang, Rui Nie, Hao Chen*, Haiying Wang, and Tong Xu

China University of Mining and Technology, China

A dual-rotor switched reluctance motor is proposed in this paper. The structure and working principle of the motor are introduced in detail. The structural parameters have great influence on the performance of the motor, so sensitivity analysis of several important structural parameters to the output torque is carried out based on the two-dimensional finite element method, which improves the average torque of the rotor in the outer air gap. Additionally, the performance of the motor with various pole distributions is analyzed and compared. The results show that when the magnetic polarity distribution of the outer stator is NSNSNSNSNSNS and the magnetic polarity distribution of the inner rotor is NSNSNS, the motor has the best performance. The torque of the motor is compared with that of the traditional single-rotor switched reluctance motor. It shows that the performance of the motor proposed in this paper is better.

Keywords : switched reluctance, dual rotors, motor electromagnetic design, electromagnetic torque

1. Introduction

Switched reluctance motor (SRM) drive has the well applied foreground on electric vehicles because of the firm structure in motor and the power converter, the high starting torque with low starting current, the high fault tolerant capability, and operation at four quadrants easily [1-7]. There are conventional inner rotor SRMs such as SRM with three-phase 12/8 structure [8], three-phase 6/4 structure [9-11], four-phase 8/6 structure, four-phase 16/12 structure, and so on. There are plenty of novel SRMs with axial flux [12], auxiliary windings, and permanent magnets on the stator yoke [13]. The switched reluctance generators with hybrid magnetic paths are also researched thoroughly in [14].

Nowadays, motor with dual rotors is a popular and important area with specific merits such as small volume, low weight, high efficiency, and easy speed-governing. The dual rotors induction motor and the dual rotors permanent-magnet motor had been developed in hybrid electric vehicle applications. In order to drive two counter-rotating propellers of a cylindrical under water vehicle, a counter-rotating dual rotor permanent magnet synchronous motor is proposed in [15]. With the aim of pulsating torque reduction, a consideration is carried out in [16] on rotor skewing arrangements of a dual rotor axial flux induction motor. An axial flux permanent magnet synchronous generator with coreless stator and dual rotors is proposed in [17], and a 2-D analytical method is presented to calculate the back EMF of this motor. Novel SRM with dual rotors can also be developed for hybrid electric vehicle drive [18-20].

In this paper, a dual-rotor SRM (DR-SRM) is designed by means of finite-element method (FEM). The structure parameters optimization and the selection of polarity distribution of outer-stator and inner-rotor have been performed. Section II gives the structure of DR-SRM. Section III gives the mathematical models. Section IV presents the optimization of structure parameters. Section V presents the comparison of average torque of DR-SRM in different polarity distribution patterns of outer-stator and inner-rotor. The paper is concluded with section VI.

2. Structure of the DR-SRM

DR-SRM is a new type of structure device developed from traditional single-stator single-rotor SRM. It is

*Corresponding author: Tel: +86-13013993107
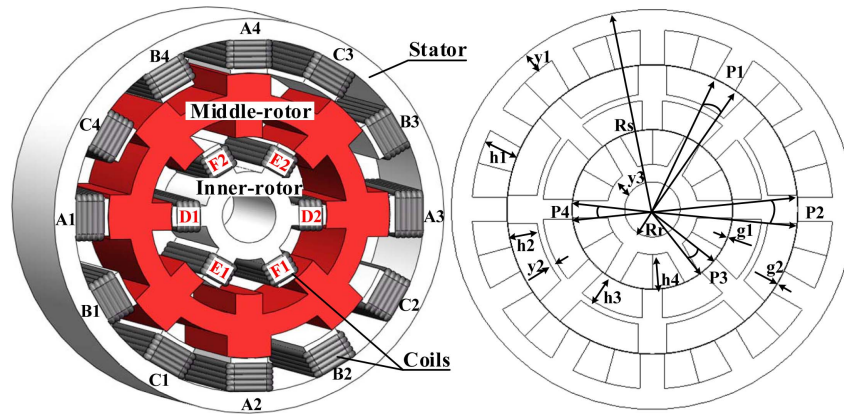Fax: +86-516-83592000, e-mail: hchen@cumt.edu.cn

Fig. 1. (Color online) Sketch structure and geometric parameters of DR-SRM.

realized by adding rotor and changing the structure of stator and rotor. The schematic structure and geometric parameters of DR-SRM are shown in Fig. 1. As shown in Fig. 1, DR-SRM consists of an outer stator, a middle rotor and an inner rotor. The middle rotor is doubly salient, windless, and has eight rotor teeth both inside and outside. The outer stator has 12 stator poles and the inner rotor has 6 rotor teeth. The winding is placed on the outer stator and the inner rotor. In this kind of motor, by increasing the number of rotors, two mechanical ports and two electrical ports are formed, and two coupled fields are generated. Therefore, better performance of the DR-SRM can be expected.

3. Mathematical Model

There are two airgaps of dual rotor SRM that can affect each other when the motor is operated, so both the outer stator winding current and the inner rotor winding current should be taken into consideration when the mathematical model of dual rotor SRM is established. The flux linkage is a function of current and rotor position angle, and the inductance is a function of current and rotor position angle as well. On outer-stator, the mutual inductances of phases are smaller than each phase's self-inductance, so the mutual inductances of windings on outer stator is negligible. There is a middle rotor between the outer stator and the inner rotor. In the design of motor dimensions, the outer stator and the inner rotor will be deliberately designed so that the flux linkage closure curves almost do not intersect and have little influence on each other. Therefore, the mutual inductance between the outer stator and the inner rotor also can be neglected. However, the mutual inductance between phases on outer stator and phases on inner rotor cannot be neglected.

The flux linkage equations of three phase dual rotors

SRM can be described as the following matrix:

$$\begin{bmatrix} \psi_1 \\ \psi_2 \end{bmatrix} = \begin{bmatrix} L_1 & L^{'} \\ L^{'} & L_2 \end{bmatrix} \begin{bmatrix} i_1 \\ i_2 \end{bmatrix} \tag{1}$$

The flux linkage vectors are:

$$\begin{cases} \psi_1 = (\psi_{1A}, \psi_{1B}, \psi_{1C})^T \\ \psi_2 = (\psi_{2D}, \psi_{2E}, \psi_{2F})^T \end{cases} \tag{2}$$

The current vectors are:

$$\begin{cases} i_1 = (i_{1A}, i_{1B}, i_{1C})^T \\ i_2 = (i_{2D}, i_{2E}, i_{2F})^T \end{cases} \tag{3}$$

The inductance vectors are:

$$\begin{cases} L_1 = [L_{1A}(i_{1A}, \theta_1), L_{1B}(i_{1B}, \theta_1), L_{1C}(i_{1C}, \theta_1)]^T \\ L_2 = [L_{2D}(i_{2D}, \theta_2), L_{2E}(i_{2E}, \theta_2), L_{2F}(i_{2F}, \theta_2)]^T \end{cases} \tag{4}$$

Where Ψ_{1A}, Ψ_{1B} and Ψ_{1C} are the flux linkage of phase A, phase B and phase C in outer stator, respectively. Ψ_{2D}, Ψ_{2E} and Ψ_{2F} are the flux linkage of D phase, E phase and F phase in inner rotor, respectively. i_{1A}, i_{1B} and i_{1C} are the winding current of phase A, phase B and phase C, respectively. i_{2D}, i_{2E} and i_{2F} are the winding current of phase D, phase E and phase F, respectively. L_{1A}, L_{1B} and L_{1C} are the self-inductance of phase A, phase B and phase C, respectively. L_{2D}, L_{2E} and L_{2F} are the self-inductance of phase D, phase E and phase F, respectively. θ_1 is relative position angle of stator pole axis and middle rotor pole axis, θ_2 is relative position angle of middle rotor pole axis and inner rotor pole axis. The subscript "1" means that the parameter belongs to outer motor and the subscript "2" means that the parameter belongs to inner motor.

The mutual inductance of the windings in outer-stator and inner-rotor is a function of the angle between the axis of A phase windings and D phase windings which is set as α:

$$L' = \begin{Bmatrix} L_{12}\cos\alpha & L_{12}\cos(\alpha+90°) & L_{12}\cos(\alpha-90°) \\ L_{12}\cos(\alpha-90°) & L_{12}\cos\alpha & L_{12}\cos(\alpha+90°) \\ L_{12}\cos(\alpha+90°) & L_{12}\cos(\alpha-90°) & L_{12}\cos\alpha \end{Bmatrix} \quad (5)$$

Where L_{12} is the amplitude of the mutual inductance L'.

The torque of the middle-rotor T_m and the torque of the inner-rotor T_i can be expressed by the following equation.

$$\begin{cases} T_m = \dfrac{\partial W_1'}{\partial\theta_1} = \dfrac{\partial(\int\psi_1 di_1)}{\partial\theta_1} \\ T_i = \dfrac{\partial W_2'}{\partial\theta_2} = \dfrac{\partial(\int\psi_2 di_2)}{\partial\theta_2} \end{cases} \quad (6)$$

where W_1' is the co-energy produced by phase A, phase B and phase C, W_2' is the co-energy produced by phase D, phase E and phase F.

The mechanical motion equation of both rotors are as follows.

$$\begin{cases} T_m - T_{L1} = J_1\dfrac{d^2\theta_1}{dt} + D\omega_1 \\ T_i - T_{L2} = J_2\dfrac{d^2\theta_2}{dt} + D\omega_2 \end{cases} \quad (7)$$

where, J_1 and J_2 are the moments of inertia of middle rotor and inner rotor, respectively, ω_1 is the angular velocity of middle rotor, ω_2 is the angular velocity of inner rotor, D is the friction coefficient, and T_{L1} and T_{L2} are the load torques of middle rotor and inner rotor.

The greater the output torque of the motor, the greater the load can be dragged and applied to more industrial and military fields. Therefore, this paper is devoted to designing new structure and optimizing motor to improve its output torque.

4. Sensitivity Analysis

The geometric parameters of DR-SRM are shown in Fig. 1. Outer radius R_s of outer-stator and laminated thickness of motor L are limited by the application space. Inner radius R_r of inner-rotor is limited by mechanical intensity of the shaft. The minimum airgap thickness is limited by manufacture technics. Hence, the optimization is conducted in the situation that the stator outer radius is 145 mm, the laminated thickness of DR-SRM is 170 mm, the inner-rotor inner radius is 20 mm, the outer airgap δ1 is 0.4 mm, and the inner airgap δ2 is 0.4 mm.

4.1. Different inner-rotor pole-arc coefficient

As shown in Fig. 2, while inner-rotor pole-arc coefficient P_4 increases from 0.250 to 0.370, the average torque of middle-rotor in the outer airgap increases from 95.676
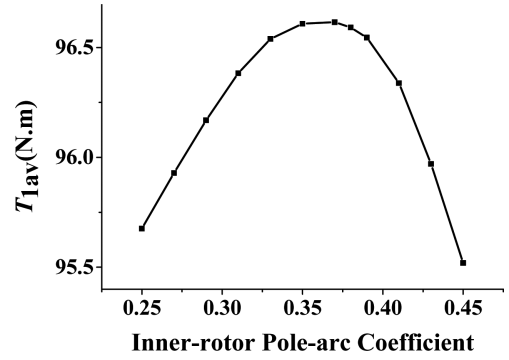

Fig. 2. Different inner-rotor pole-arc coefficient.

N.m to 96.615 N.m since the difference of maximum phase inductance and minimum phase inductance of the outer motor is enhanced with increasing the inner-rotor pole-arc coefficient. While inner-rotor pole-arc coefficient P_4 increases from 0.370 to 0.450, the average torque of middle-rotor in the outer airgap decreases from 96.615 N.m to 95.519 N.m. Hence, the final inner-rotor pole-arc coefficient is set as 0.370.

4.2. Different inner-rotor yoke thickness

As shown in Fig. 3, while inner-rotor yoke thickness y_3 increases from 7.6 mm to 14.6 mm, the average torque of middle-rotor in the outer airgap increases from 96.440 N.m to 96.715 N.m since the ferric reluctance in inner-rotor yoke decreases which results in the increase of the main flux at the same excitation. Hence the final dimension of inner-rotor yoke thickness is set as 12.6 mm with considering the installation of inner-rotor coils smoothly in the inner-rotor slot.

4.3. Different outer-stator pole-arc coefficient

As shown in Fig. 4, while outer-stator pole-arc coefficient P_1 increases from 0.260 to 0.320, the average torque of middle-rotor in the outer airgap rises from 147.445 N.m to 154.515 N.m since the difference between maximum
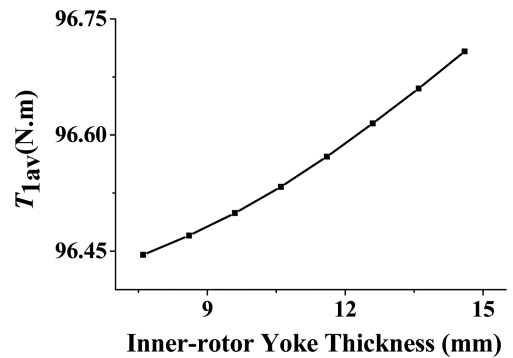

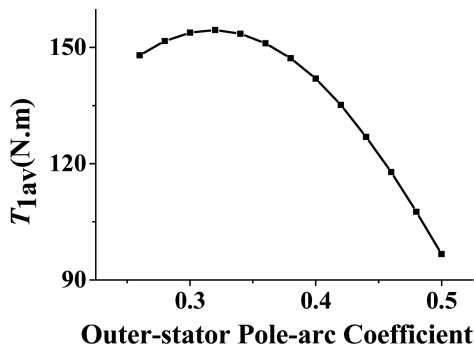**Fig. 3.** Different inner-rotor yoke thickness.

Fig. 4. Different outer-stator pole-arc coefficient.

Fig. 6. Different middle-rotor inner tooth pole-arc coefficient.
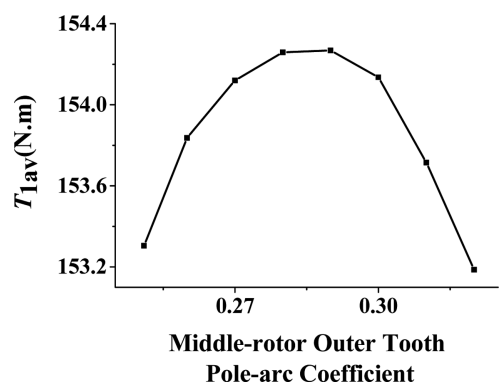
Fig. 7. Different middle-rotor outer tooth pole-arc coefficient.

phase inductance and minimum phase inductance of the outer motor increases. While outer-stator pole-arc coefficient P_1 increases from 0.320 to 0.500, the average torque of middle-rotor in the outer airgap declines from 154.515 N.m to 96.671 N.m. Hence, the final outer-stator pole-arc coefficient is set as 0.320.

4.4. Different outer-stator yoke thickness

As shown in Fig. 5, when the outer-stator yoke thickness y_1 increases from 11.0 mm to 18.0 mm, the average torque of middle-rotor in the outer airgap increases from 150.450 N.m to 155.800 N.m since the ferric reluctance in outer-stator yoke decreases which results in the increase of the main flux at the same excitation. The final dimension of outer-stator yoke thickness is set as 15.0 mm with considering the installation of outer-stator coils smoothly in the outer-stator slot.

4.5. Different middle-rotor tooth pole-arc coefficient

After the optimization of inner-rotor and outer-stator, the middle-rotor inner tooth pole-arc coefficient P_3 and the middle-rotor outer tooth pole-arc coefficient P_2 are to be optimized.

As shown in Fig. 6, when the middle-rotor inner tooth pole-arc coefficient P_3 increases from 0.277 to 0.310, the
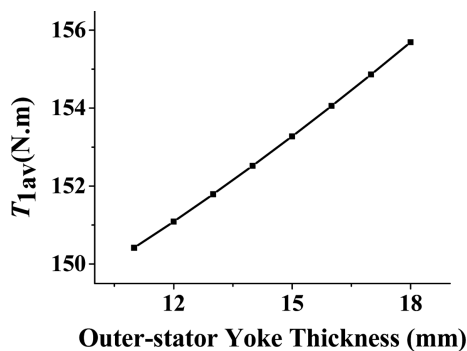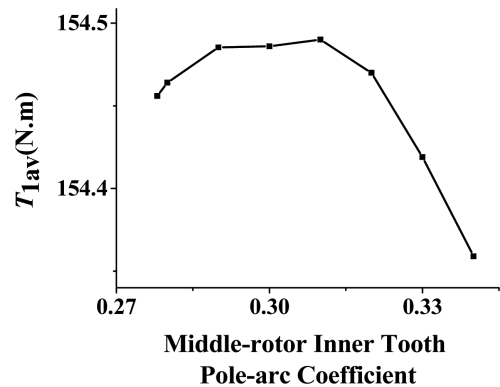
average torque of middle-rotor in the outer airgap increases from 154.455 N.m to 154.490 N.m. When the middle-rotor inner tooth pole-arc coefficient P_3 increases from 0.310 to 0.340, the average torque of middle-rotor in the outer airgap decreases quickly. The final middle-rotor inner tooth pole-arc coefficient is set as 0.310.

As shown in Fig. 7, when the middle-rotor outer tooth pole-arc coefficient P_2 increases from 0.251 to 0.290, the average torque of middle-rotor in the outer airgap increases. While the middle-rotor outer tooth pole-arc coefficient P_2 increases from 0.290 to 0.320, the average torque of middle-rotor in the outer airgap decreases. The final middle-rotor outer tooth pole-arc coefficient is set as 0.290.

4.6. Different middle-rotor yoke thickness

As shown in Fig. 8, when the middle-rotor yoke thickness y_2 increases from 2.6 mm to 4.6 mm, the average torque of middle-rotor in the outer airgap goes up as well because the ferric reluctance in middle-rotor yoke decreases which results in the increase of the main flux at the same excitation. But while the middle-rotor yoke thickness y_2 increases from 4.6 mm to 18.6 mm, the average torque of middle-rotor falls quickly. The final middle-rotor yoke thickness is set as 4.6 mm.
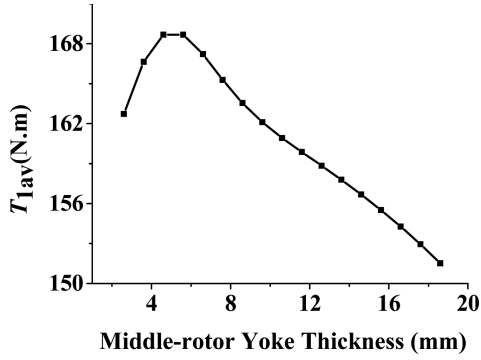

Fig. 5. Different outer-stator yoke thickness.

Fig. 8. Different middle-rotor yoke thickness.

The height of the outer-stator pole h_1 is set as 25 mm with considering the installation of the outer-stator coils smoothly in outer-stator slot and the effective radius for torque of middle-rotor in the outer airgap. The height of the inner-rotor pole h_4 is set as 25 mm with considering the installation of inner-rotor coils smoothly in the inner-rotor slot and the effective radius for torque of middle-rotor in the inner airgap. The height of the middle-rotor inner tooth h_3 is the same as that of the middle-rotor outer tooth h_2 in order to balance the difference of maximum reluctance and minimum reluctance in inner motor and the difference of maximum reluctance and minimum reluctance in outer motor. So

$$h_2 = h_3 = \frac{R_S - y_1 - h_1 - \delta_1 - (R_r + y_3 + h_4 + \delta_2) - y_2}{2} \quad (8)$$

4.7. Comparison of torque on DR-SRM and single inner rotor SRM

A final geometry size of DR-SRM is given in Table 1. According to the optimized dimension table, the two-dimensional finite element analysis of DR-SRM is carried out and compared with the traditional single stator and single rotor SRM with the same specifications. When DR-SRM and traditional SRM have the same stator outer diameter, the same stack thickness, the same stator inner diameter, the same air gap size and the same excitation of stator windings, the rotor torque in the outer air gap of DR-SRM and the torque of traditional three-phase 12/8 single-inner rotor SRM are calculated and illustrated in Fig. 9. As shown in Fig. 9, the overall amplitude and mean of DR-SRM's torque are larger than that of traditional single-rotor Internal-Rotor SRM.

5. Different Polarity Distribution

The coils forming one phase winding can be connected in different ways, which makes outer-stator and inner-

Table 1. Geometry size of DR-SRM.

| Name	Parameters	Size
Outer-stator outer radius	R_S	145 mm
Laminated thickness	L	170 mm
Inner-rotor inner radius	R_r	20 mm
Outer airgap	δ_1	0.4 mm
Inner airgap	δ_2	0.4 mm
Inner-rotor pole-arc coefficient	P_4	0.370
Inner-rotor yoke thickness	y_3	12.6 mm
Outer-stator pole-arc coefficient	P_1	0.320
Outer-stator yoke thickness	y_1	15.0 mm
Middle-rotor inner tooth pole-arc coefficient	P_3	0.310
Middle-rotor outer tooth pole-arc coefficient	P_2	0.290
Middle-rotor yoke thickness	y_2	4.6 mm
Height of the outer-stator pole	h_1	25 mm
Height of the inner-rotor pole	h_4	25 mm
Height of the middle-rotor inner tooth	h_3	21.0 mm
Height of the middle-rotor outer tooth	h_2	21.0 mm
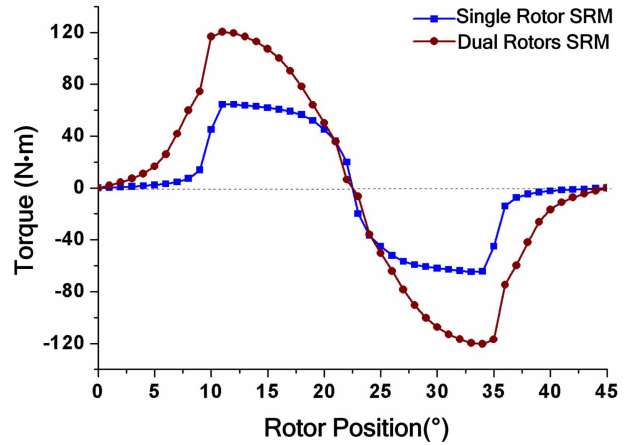
Fig. 9. (Color online) Calculated torque at one rotor period.

rotor have different polarity. The different polarity distribution leads to different magnetic field distribution, which has a great effect on the electromagnetic torque of DR-SRM.

The polarity distribution of outer-stator is set as NSNSNSNSNSNS (outer-stator pattern I), and the polarity distribution of inner-rotor has three kinds of distribution patterns which are respectively NSNSNS, NNNSSS and NNNNNN. The polarity distribution and the magnetic-flux path distribution with phase A and phase E excited are shown in Fig. 10. The calculated average torque of middle-rotor in the outer airgap is given in Table 2.

The polarity distribution of outer-stator is set as NNNNNNSSSSSS (outer-stator pattern II), and the polarity distribution of inner-rotor has three kinds of distribution patterns which are respectively NSNSNS,
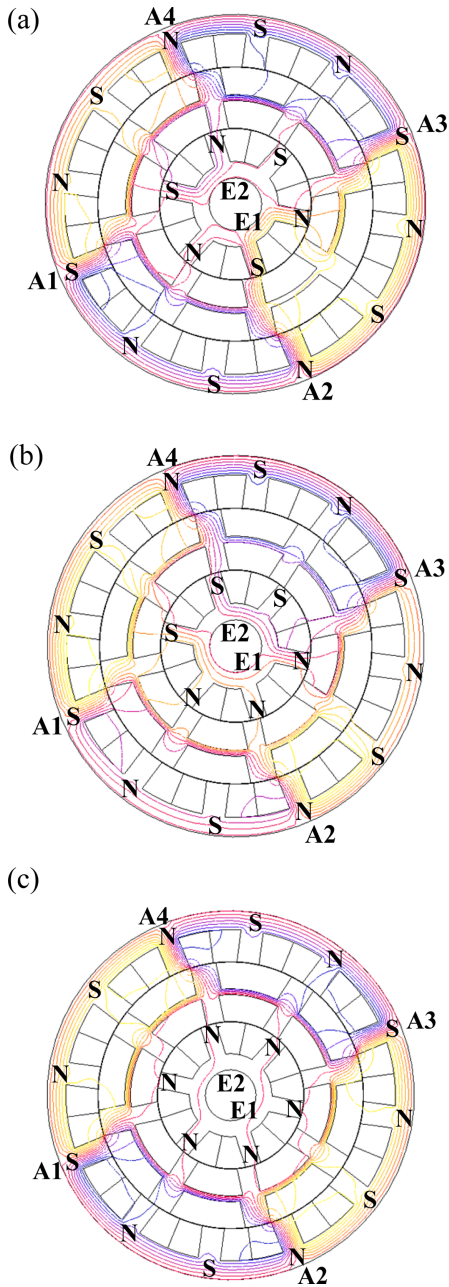
Fig. 10. (Color online) Polarity distribution and isolines of flux density on outer-stator pattern I. (a) NSNSNS (b) NNNSSS (c) NNNNNN.
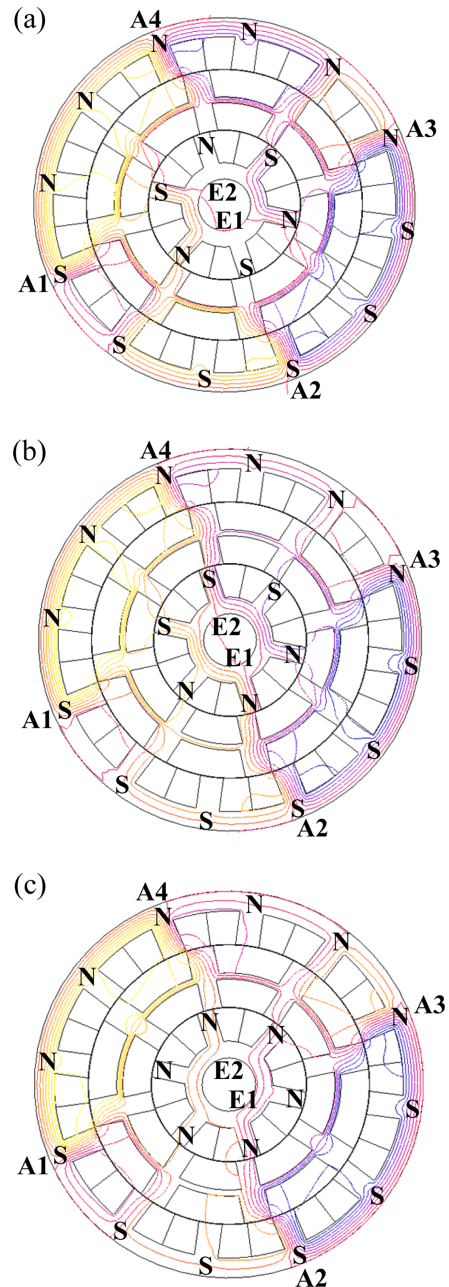

Fig. 11. (Color online) Polarity distribution and isolines of flux density on outer-stator pattern II. (a) NSNSNS (b) NNNSSS (c) NNNNNN.

NNNSSS and NNNNNN. The polarity distribution and the magnetic-flux path distribution with A phase and E phase excited are shown in Fig. 11. The calculated average torque of middle-rotor in the outer air-gap is given in Table 2.

The polarity distribution of outer-stator is set as SSSSSSSSSSSS (outer-stator pattern III), and the polarity distribution of inner-rotor has four kinds of distribution patterns which are respectively NSNSNS, NNNSSS,

NNNNNN and SSSSSS. The polarity distribution and the magnetic-flux path distribution with A phase and E phase excited are shown in Fig. 12. The calculated average torque of middle-rotor in the outer airgap is given in Table 2.

It is shown that the average torque of middle-rotor in the outer airgap with NSNSNSNSNSNS polarity distribution of outer-stator and NSNSNS polarity distribution of inner-rotor is the largest since the magnetic-flux path in
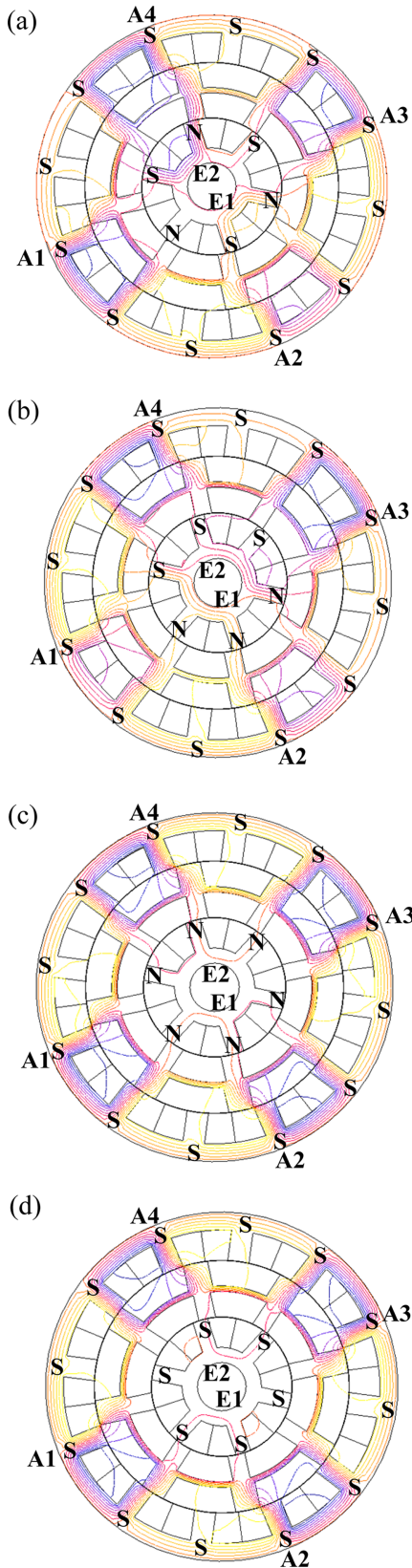
Fig. 12. (Color online) Polarity distribution and isolines of flux density on outer-stator pattern III. (a) NSNSNS (b) NNNSSS (c) NNNNNN (d) SSSSSS

Table 2. Calculated average torque on outer-stator in different patterns.

Polarity distribution of outer-stator	Polarity distribution of inner-rotor	T_{1av} (N.m)
NSNSNSNSNSNS	NSNSNS	139.389N .m
	NNNSSS	135.881 N.m
	NNNNNN	129.105 N.m
NNNNNNSSSSSS	NSNSNS	133.322 N.m
	NNNSSS	122.014 N.m
	NNNNNN	111.361 N.m
SSSSSSSSSSSS	NSNSNS	53.679 N.m
	NNNSSS	49.012 N.m
	NNNNNN	42.121 N.m
	SSSSSS	41.838 N.m

airgap and in ferric core is the shortest. This pattern is selected. It can be reasonably inferred from the comparative analysis results of various pole distribution modes that the motor with shorter magnetic path is more likely. This conclusion can be extended to research about the motors with more poles, dual rotors and dual stators.

6. Conclusion

In this paper, a DR-SRM with an outer-stator, a middle-rotor and an inner-rotor has been introduced. The structure geometry parameters optimization and selection of polarity distribution of DR-SRM are conducted. The average torque of middle rotor in the outer airgap contributing to the main parts of energy conversion with different geometry sizes of stator and rotors is calculated. Furthermore, average torque of middle rotor with different polarity distribution patterns of outer-stator and inner-rotor are calculated. The final geometry size, the polarity distribution pattern of outer-stator and inner-rotor are designed and optimized for enhancing the average torque of middle-rotor in the outer airgap at certain volume. The comparison results of torque on the dual rotors SRM and the conventional single inner rotor SRM show that the dual rotors SRM has much better electromagnetic torque performance than conventional single inner rotor SRM.

Acknowledgements

References

[1] C. Zhang, K. Wang, and S. Zhang, IEEE Trans. Appl. Supercond. **26**, 7 (2016).

[2] J. H. Lee, Y. H. Lee, and D. H. Kim, IEEE Trans. Appl. Supercond. **12**, 1 (2002).

[3] X. Liu, J. Gao, S. Huang, and K. Lu, IEEE Trans. Magn. **53**, 6 (2017).

[4] H. Chen, G. Han, and W. Yan, IEEE Trans. Appl. Supercond. **26**, 4 (2016).

[5] J. F. Pan, N. C. Cheung, and Y. Zou, IEEE Trans. Magn. **48**, 11 (2012).

[6] K. Zhang, X. Huang, and J. Zhang, IEEE Trans. Appl. Supercond. **26**, 7 (2016).

[7] X. Cao and Z. Deng, IEEE Trans. Appl. Supercond. **20**, 3 (2010).

[8] C. Moron, A. Garcia, E. Tremps, and J. A. Somolinos, IEEE Trans. Magn. **48**, 4 (2012).

[9] G. Li, J. Ojeda, S. Hlioui, E. Hoang, M. Lecrivain, and M. Gabsi, IEEE Trans. Magn. **48**, 6 (2012).

[10] H. Torkaman, E. Afjei, and P. Yadegari, IEEE Trans. Magn. **48**, 8 (2012).

[11] J. Li, X. Song, and Y. Cho, IEEE Trans. Magn. **44**, 11 (2008).

[12] A. Labak and N. C. Kar, IEEE Trans. Magn. **49**, 8 (2013).

[13] Y. Hasegawa, K. Nakamura, and O. Ichinokura, IEEE Trans. Magn. **48**, 11 (2012).

[14] X. D. Xue, K. W. E. Cheng, Y. J. Bao, P. L. Leung, and N. Cheung, IEEE Trans. Magn. **48**, 11 (2012).

[15] G. W. Liu, G. Qiu, S. Jin, and F. Zhang, IEEE Trans. Appl. Supercond. **28**, 3 (2018).

[16] A. Nobahari, A. Darabi, and A. Hassannia, IET Electr. Power Appl. **12**, 4 (2018).

[17] J. Ikram, N. Khan, Q. Junaid, S. Khaliq, and B. Kwon, J. Magn. **22**, 257 (2017).

[18] M. Aryanezhad, 2015 30th International Power System Conference (PSC), Tehran, (2015) pp 54-59.

[19] T. Guo, N. Schofield, and A. Emadi, IEEE Trans. Energy Conver., **31**, 4 (2016).

[20] W. Yang, L. Quan, X. Zhu, D. Chen, and Y. Du, 2010 International Conference on Electrical Machines and Systems, (2010) pp 829-833.